

# The thermal characteristics of ACCR lines as a function of wind speed – an analytical approach

Marek ZARĘBA\* and Jerzy GOŁĘBIOWSKI

Faculty of Electrical Engineering, Białystok University of Technology, ul. Wiejska 45D, 15-351 Białystok, Poland

**Abstract.** The paper has investigated the effect of wind speed on selected thermal characteristics of the contemporary ACCR line. As wind speed functions, heating curves, stationary temperature profiles, steady-state current ratings and thermal time constants, have been determined. The composite core (Al–Al<sub>2</sub>O<sub>3</sub>) and the Al–Zr alloy braid were modeled as porous solids. As a result, the physical model is composed of a solid cylinder and a hollow cylinder with different material parameters of the above-mentioned elements. The mathematical model was formulated as the boundary-initial problem of the parabolic heat equation. The problem was solved by the state-superposition of and variable-separation method. On this basis, a computer program was developed in the Mathematica 10.4 environment and the velocity characteristics sought for were plotted. The results obtained analytically were positively verified by the finite-element method in the NISA v.16 environment. The physical interpretation of the determined characteristics has been given.

**Key words:** wind speed; transient and steady temperature field; ACCR line; mathematical modeling.

## 1. INTRODUCTION

In overhead power lines of the new generation, bearing steel cores (e.g., in ACSR, ACSS) have been substituted with composite cores (e.g., in ACCR, ACCC). The meaning of the abbreviations used is as follows: ACSR – aluminum conductor steel reinforced, ACSS – aluminum conductor steel supported, ACCR – aluminum conductor composite reinforced, ACCC – aluminum conductor composite core. The composite core in ACCR is formed from aluminum oxide microfibers embedded in high-purity aluminum (Al–Al<sub>2</sub>O<sub>3</sub>). It is about 2.4 times lighter than the steel core. At the same time, the strength to weight ratio is approx. 2.6 times greater than for steel strands. Moreover, the coefficient of thermal expansion of the Al–Al<sub>2</sub>O<sub>3</sub> material is about two times smaller than that of steel [1, 2]. These are very much desirable properties which, at the same time, reduce the sag of the line and increase the resistance to mechanical load (such as icing or wind).

Contemporary lines also have a different material of the braid. In the case of conventional aluminum-steel lines, this is either hard aluminum or an aluminum-magnesium-silicon (Al–Mg–Si) alloy. These are materials of low thermal resistance (with a sustained maximum temperature of approx. 80°C.) In the ACCR line, the braid is made of an aluminum-zirconium (Al–Zr) alloy. The latter element eliminates the risk of braid annealing (softening). As a result, the maximum operating temperature is 210°C (and under overload conditions, even 240°C for 1000 hours in total) [1, 2]. Due to the above factors, the electrical current carrying capacity (ampacity) of the ACCR

is even twice as high as that of the ACSR, with a smaller sag of a line of the identical diameter [1, 2]. Because of the similar dimensions of ACCR and ACSR, the same supporting structures can be used (thus avoiding the need for constructing new towers or increasing the height of existing ones). For the above-mentioned reasons, the analysis of phenomena occurring in the ACCR line meets both the current and prospective needs of electrical power engineering. The temperature of the power line is one of its most important operating parameters.

The distribution of the temperature field in the ACCR line depends heavily on the speed  $U$  of ambient air (wind) [3, 4]. At a high wind speed, the intensity of forced convection (cooling) increases. In such conditions, it is possible to increase the intensity  $I$  of transmitted current without the risk of exceeding the maximum operating temperature of the line. For increasing  $I$ , systems for monitoring the weather (among others wind speed), conductor temperature, stresses and sags are used [5]. Another method for determining the wind speed is by the statistical processing of historical data in the geographical region under consideration [6]. The most endangered segments (i.e., those with light wind) are also identified [7]. Papers [3, 5, 7] are devoted to classic ACSR lines in a steady state. All of the mentioned articles have a common physical basis. It is the balance of thermal powers drawn up in conformance to standards IEEE [8] or CIGRE [9]. In a steady state, the sum of Joule's and solar radiation powers is equal to the sum of infrared radiation and convection powers. The effect of air (wind) speed  $U$  reveals itself in the latter of the aforementioned components. Namely, the convection heat transfer coefficient  $\alpha_c$  is heavily dependent on  $U$  (through the Nusselt number  $Nu$  and the Reynolds number  $Re$  [10]). From the balance, the steady-state current rating (or current carrying capacity) can be determined

\*e-mail: [m.zareba@pb.edu.pl](mailto:m.zareba@pb.edu.pl)

Manuscript submitted 2021-10-25, revised 2022-01-11, initially accepted for publication 2022-02-09, published in June 2022.

as a function of air speed,  $I = f_1(U)$ . Much more difficult is to determine the conductor temperature  $T$  as a function of  $U$ . This is due to the fourth power of  $T$  in the radiation component and other nonlinearities. In this situation, it is necessary to use iteration methods that do not lead to a closed form of the solution. For this reason, the relationship  $T = f_2(U)$  has often been examined experimentally in a steady state. The results of studies by several authors are presented in [4] and [11] in the form of experimental characteristics  $T = f_2(U)$  (for the transverse and longitudinal wind speeds relative to the conductor). Using experimental methods, transient states in the ACSR line [12] were also examined. Study [12] describes two complex measuring stands designed for testing stationary air and forced convection in a wind tunnel. Solar radiation was omitted. The experiment results made it possible to determine the effect of current and wind speed on the transient conductor temperature and the rate of its variation. The same relationships were examined in the ACCC line, though using numerical methods [13]. In [13], commercial software based on the finite element method (FEM) [14, 15] was used. In addition to the wind speed  $U$ , the effect of conductor surface emissivity  $\varepsilon$  has also been discussed, though the solar radiation and the skin effect have been omitted.

A more comprehensive review of the relevant literature and the above-cited studies has shown that numerical (including iterative) and experimental methods predominate in the studies of the effect of wind speed on the distribution of the temperature of overhead power lines. The lack of advanced analytical methods is conspicuous. The present article partially fills this gap.

The subject of the present study is the determination of selected characteristics and parameters of the contemporary ACCR line as a function of wind speed. The system belongs to a new generation of HTLS (High Temperature Low Sag) conductors. The respective mathematical model was solved by the variable-separation method [16]. Its main advantage are results in the form of formulas. They support the engineer's intuition and facilitate the physical interpretation and discussion on the effect of individual parameters. Analytical formulas also enable the quick estimation of the field at selected points of space-time, the finding of scaling laws and testing of numerical computations on asymptotic examples.

The following characteristics of the ACCR line have been determined as a function of air (wind) speed:

- heating curves,
- steady-state current ratings (or current carrying capacity),
- thermal time constants, and
- stationary temperature profiles.

The second of the above-mentioned parameters is crucial for the thermal safety of the system. The first and thirds characteristics are important in the analysis of transient states (e.g., when switching the line on and off, changing the load, with discontinuous operation, etc.). Stationary temperature profiles, on the other hand, are used for the assessment of the correctness of sustained operation. In the authors' opinion, an original feature of the paper is the determination of the above-mentioned characteristics by analytic means. The ACCR line was modeled as a system with distributed parameters (i.e., it was decided not to

assume the isothermal volume). Moreover, solar radiation and the skin effect were taken into account.

The structure of the paper is made up of the following steps of the analysis of the ACCR line:

- formulating the physical model (or the set of simplifying assumptions),
- formulating the mathematical model in the form of a boundary-initial problem for the heat equation,
- solving the mathematical model (determining the stationary field distributions, separating the variables in the heat equation, constructing the eigenvalues equation, reducing the number of eigenfunctions coefficients, and using the condition of the orthogonality of radial coordinate eigenfunctions),
- determining the previously mentioned thermal characteristics of the ACCR line as a function of wind speed, and
- formulating the final conclusions concerning the thermal phenomena in the ACCR line and the employed computation techniques.

## 2. PHYSICAL MODEL OF THE ACCR LINE

Figure 1 shows the cross-section of an ACCR line. The core ( $r \leq a$ , index 1) contains aluminum-matrix (Al-Al<sub>2</sub>O<sub>3</sub>) composite wires. The outer strands ( $a \leq r \leq b$ , index 2) are composed of temperature-resistant aluminum-zirconium (Al-Zr) alloy. The following designations are adopted above:  $r$  is the radial coordinate,  $a$  denotes the core radius, and  $b$  is the outer radius of the conductor. The entire system is helically stranded. The space between the wires is filled with air. For this reason, the system under examination was considered a porous body, and its equivalent parameters were determined following the rules provided in references [17, 18]. For this purpose, the knowledge of the active cross-sections of the composite,  $S_1 < \pi a^2$ , and of the alloy,  $S_2 < \pi(b^2 - a^2)$ , was utilized. It was assumed that the braid surface area ( $r = b$ ) was oxidized to a medium degree (i.e., the emissivity  $\varepsilon = 0.5$ ).

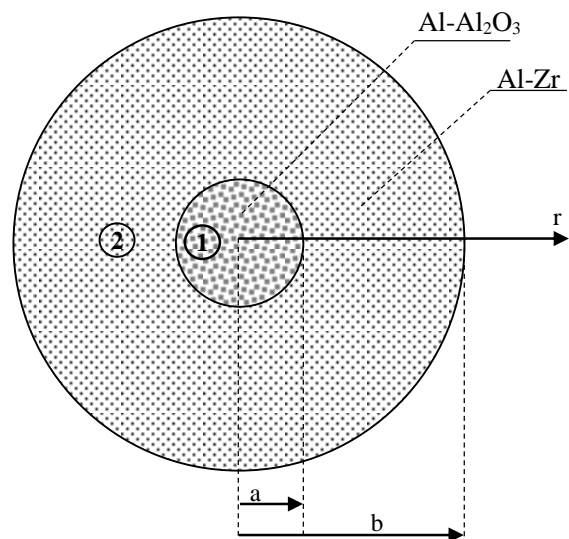


Fig. 1. Cross-section of the ACCR conductor

The thermal field is generated from the moment of switching on current with a frequency of  $f$  and a root-mean-square value of  $|I|$ . The current  $I$  separates into components:  $I_1$  in the core and  $I_2$  in the braid. The components  $I_1, I_2$  are determined using a current divider.

Solar radiation can be included for by using the surface density of its power ( $\text{W/m}^2$ ) [8, 9] or the temperature of the sun sensor [19, 20]. In this study, the latter method was used. The simplest sensor is a replica of the conductor [19, 20] positioned next to the actual system.  $T_s$  was assumed to represent the temperature of the entire volume of the replica heated up by solar radiation. So,  $T_s$  is also the temperature of the conductor before the power supply is switched on (that is for  $t < 0$ ). The replica is never charged with electricity – there is only the solar input. For this reason, a constant value of replica temperature,  $T_s$ , is assumed (even when the actual line is on). The increment  $T_s - T_a$  is a measure of the intensity of solar radiation. The  $T_a$  is the constant ambient temperature.

The cooling of the system was modeled using the total heat transfer coefficient,  $\alpha$ . It is the sum [10] of the convection,  $\alpha_c$ , and radiation,  $\alpha_r$ , coefficients. The first component considers [21] – Table 3, *inter alia*, wind speed,  $U$ ; conductor diameter,  $2b$ ; and the thermal conductivity and kinematic viscosity of air at the average temperature in the boundary layer. Air parameters at a given temperature were taken from relevant tables [10]. The angle  $\Theta$  between the conductor axis and the wind direction is also of great importance. Usually, the normal (cross) direction of flow relative to the line has been assumed ( $\Theta = 90^\circ$ ). Besides [21], there are many other  $\alpha_c$  models [4]. In the case of forced convection ( $U > 0$ ), various functions of the Reynolds number are the  $\alpha_c$  coefficient. For  $U = 0$  (free convection), the  $\alpha_c$  coefficient depends on the Rayleigh number. In the present paper, the references [21]– Table 3 (for  $U > 0$ ) and [10] (for  $U = 0$ ) have been used.

In turn, the  $\alpha_r$  radiation component [10] depends, among other things, on the emissivity  $\varepsilon$  and on the average temperature of the environment and conductor surface.

The most important elements of the physical model are the following assumptions:

- the cylindrical coordinate system is adopted. As a result, the symmetries of the ACCR line and the coordinate system are the same,
- the length of the line is much greater than its outer diameter. As a result, the thermal field does not depend on the “ $z$ ” coordinate along the line axis. This also means the omission of edge phenomena for large values of  $|z|$ ,
- the surface of the line ( $r = b$ ) uniformly gives up heat to the environment. In such a case, the thermal field does not depend on the angular coordinate,  $\varphi$ , which means that an axial symmetry occurs,
- the geometry of the line and the previous assumptions allow the approximation of the temperature field with the function of the radial coordinate,  $r$ , and time,  $t$ ,
- all thermo-physical parameters have been averaged in the temperature variation interval. This means the linearization of the system, thus enabling the superposition principle to be used.

### 3. MATHEMATICAL MODEL OF THE ACCR LINE THERMAL FIELD

Temperature increments  $v_i(r, t)$  and  $T_s - T_a$  are calculated relative to temperature  $T_a$  and are generated, respectively, by current flow and solar radiation ( $i = 1$  for  $0 \leq r \leq a$ ,  $i = 2$  for  $a \leq r \leq b$ ). According to the Electric Power Research Institute – USA [20], the above-mentioned increments can be analyzed separately. After the thermal and material parameters have been averaged out, the system is linear. The superposition of the increments results in

$$T_i(r, t) = T_s + v_i(r, t), \quad (1)$$

where  $T_i(r, t)$  denotes the space-time distribution of temperature in the  $i$ -th zone. The current-generated temperature increase  $v_i(r, t)$  above  $T_a$  is defined using the following boundary-initial problem for the heat equation [17, 22]

$$\frac{\partial^2 v_i(r, t)}{\partial r^2} + \frac{1}{r} \frac{\partial v_i(r, t)}{\partial r} - \frac{1}{\chi_i} \frac{\partial v_i(r, t)}{\partial t} = -\frac{g_i}{\lambda_i}, \quad (2)$$

where  $i = 1$  for  $0 \leq r \leq a$ ,  $i = 2$  for  $a \leq r \leq b$ . Equation (2) also follows from the assumptions presented at the end of Section 2. The following designations of the equivalent material parameters of the porous body [17, 18] in the  $i$ -th zone are adopted above:  $\chi_i = \lambda_i / (c_i \mu_i)$  is diffusivity,  $\lambda_i$  is thermal conductivity,  $c_i$  is specific heat, and  $\mu_i$  is mass density. Heat source efficiencies,  $g_i$ , are defined as follows ( $i = 1$  for  $0 \leq r \leq a$ ,  $i = 2$  for  $a \leq r \leq b$ )

$$g_i = \frac{P_i}{V_i} = \frac{R_i |I_i|^2}{V_i}, \quad \text{where} \quad (3a)$$

$$R_i = n_i k_i R_{DCi} = n_i k_i \frac{\rho_i l}{S_i}, \quad \text{where} \quad (3b)$$

$$|I_1| = |I| \frac{R_2}{R_1 + R_2}, \quad |I_2| = |I| \frac{R_1}{R_1 + R_2}, \quad (3c)$$

$$V_1 = \pi a^2 l, \quad V_2 = \pi (b^2 - a^2) l. \quad (3d)$$

In formulas (3a)–(3d), the following designations relating to the  $i$ -th zone of the length  $l$  are adopted:  $P_i$  is active power released, respectively, in the composite and in the alloy;  $V_i$  denotes the volume of the core or braid section;  $R_i$  and  $R_{DCi}$  are, respectively, the alternating-current and direct-current resistance of the section;  $|I_i|$  is the root-mean-square value of current, respectively, in the core and in the braid;  $\rho_i$  denote the resistivity of, respectively, the Al–Al<sub>2</sub>O<sub>3</sub> composite and the Al–Zr alloy at the average operating temperature;  $S_i$  is the active cross-section of, respectively, the composite and the alloy ( $S_1 < \pi a^2, S_2 < \pi (b^2 - a^2)$ );  $n_i$  are stranding (elongation) factors [23]; and  $k_i$  are skin factors [24] for mains frequency in the cylinder ( $i = 1$ ) or in the hollow cylinder ( $i = 2$ ), respectively.

The model under consideration assumes that the flow of current heats the system from the moment  $t = 0$ . The current-generated temperature increase is calculated in relation to  $T_a$  with the conductor being completely shielded against solar ra-

diation. This results in zero initial conditions in two conductor zones

$$v_i(r, t = 0) = 0, \quad (4)$$

where  $i = 1$  for  $0 \leq r \leq a$  and  $i = 2$  for  $a \leq r \leq b$ .

The outer surface of the conductor ( $r = b$ ) gives up heat by convection and radiation. This process is described by the boundary condition of the third kind (Hankel) [17, 22]

$$\left. \frac{\partial v_2(r, t)}{\partial r} \right|_{r=b} = -\frac{\alpha}{\lambda_2} v_2(r = b, t) \quad \text{for } t > 0, \quad (5a)$$

where  $\alpha$  is the total heat transfer coefficient ( $\alpha = \alpha_c + \alpha_r$ ):

$$\alpha = \begin{cases} f_3(\text{Ra}, \varepsilon) & \text{for } U = 0, \\ f_4(\text{Re}, \Theta, \varepsilon) & \text{for } U > 0. \end{cases} \quad (5b)$$

In formula (5b),  $f_3$  denotes the function of the Rayleigh number  $\text{Ra}$  and emissivity  $\varepsilon$ , while  $f_4$  is the function of the Reynolds number  $\text{Re}$ , wind angle  $\Theta$  and emissivity  $\varepsilon$ . The dependence of the total coefficient  $\alpha$  on the wind speed  $U$  is hidden in the number  $\text{Re} = (U2b)/\eta$ , where  $\eta$  denotes the kinematic viscosity of the boundary air layer at the average temperature [4, 10], [21] – Table 3.

The equivalent zones of the core and braid are closely adjacent to each other. Therefore, the conditions of the continuity of temperature and heat flux increase on the perimeter of the boundary circle,  $r = a$ , are satisfied

$$v_1(r = a, t) = v_2(r = a, t) \quad \text{for } t > 0, \quad (6a)$$

$$\lambda_1 \left. \frac{\partial v_1(r, t)}{\partial r} \right|_{r=a} = \lambda_2 \left. \frac{\partial v_2(r, t)}{\partial r} \right|_{r=a} \quad \text{for } t > 0. \quad (6b)$$

Relationships (2)–(6) form a boundary-initial problem for the transient increase of the temperature field generated by current (with perfect conductor shielding against solar radiation)

#### 4. HEATING CURVES OF THE ACCR LINE

At the first stage of analysis, the method of superposition of the steady and transient states was employed

$$v_i(r, t) = v_{is}(r) + v_{it}(r, t) \quad \text{for } i = 1, 2 \quad (7)$$

where  $v_{is}(r)$  is the steady component of the temperature increase of the  $i$ -th conductor zone ( $\lim_{t \rightarrow \infty} v_i(r, t) = v_{is}(r)$ ),  $v_{it}(r, t)$  denotes the transient component of the temperature increase of the  $i$ -th conductor zone ( $\lim_{t \rightarrow \infty} v_{it}(r, t) = 0$ ).

To formulate the boundary condition for the stationary components  $v_{is}(r)$ , a change to the function  $v_i(r, t) \rightarrow v_{is}(r)$  in (2), (5a), (6) was made. As a result of this operation, the partial derivatives will change into normal derivatives with respect to  $r$ , while with respect to time, they will zero. Then, using the formula for the derivative of the product, the notation of the left-hand side of (2) was reduced (for  $i = 1, 2$ ). After integrating

thus changed Equation (2) twice, rejecting the singular component with  $r = 0$  (for  $i = 1$ ) and determining the constants from the modified conditions (5a), (6), the following were obtained:

$$v_{1s}(r) = \frac{g_1}{4\lambda_1} (a^2 - r^2) + \frac{g_2}{4\lambda_2} (b^2 - a^2) - \frac{(g_2 - g_1)a^2}{2\alpha b} + \frac{g_2 b}{2\alpha} - \frac{(g_2 - g_1)a^2}{2\lambda_2} \ln\left(\frac{b}{a}\right) \quad \text{for } 0 \leq r \leq a, \quad (8)$$

$$v_{2s}(r) = \frac{g_2}{4\lambda_2} (b^2 - r^2) - \frac{(g_2 - g_1)a^2}{2\alpha b} + \frac{g_2 b}{2\alpha} - \frac{(g_2 - g_1)a^2}{2\lambda_2} \ln\left(\frac{b}{r}\right) \quad \text{for } a \leq r \leq b, \quad (9)$$

where  $g_1$  and  $g_2$  were determined from formulas (3).

On the other hand, the boundary-initial problem for the transient components results from (7). Relationships (2)–(6) and the boundary condition for the stationary components were also used. Finally, it is sufficient to make change in  $v_i(r, t) \rightarrow v_{it}(r, t)$  and, additionally, to substitute  $g_i = 0$  for  $i = 1, 2$  in relationships (2), (5a), (6). Only the form of (4) will change

$$v_{ii}(r, 0) = -v_{is}(r) \quad \text{for } i = 1 \text{ with } 0 \leq r \leq a \text{ and} \\ \text{for } i = 2 \text{ with } a \leq r \leq b. \quad (10)$$

So obtained homogeneous partial differential equations were solved by the (Fourier) variables separation method [16]. Accordingly, after separating the time and position variables and rejecting the singular component with  $r =$ , the following were obtained

$$v_{1t}(r, t) = \sum_{n=1}^{\infty} C_n J_0(\gamma_n r/a) e^{-\gamma_n^2 \frac{\lambda_1}{a^2} t} \quad \text{for } 0 \leq r \leq a, \quad t > 0, \quad (11)$$

$$v_{2t}(r, t) = \sum_{n=1}^{\infty} [D_n J_0(\gamma_n s r/a) + E_n Y_0(\gamma_n s r/a)] e^{-\gamma_n^2 \frac{\lambda_2}{a^2} t} \quad \text{for } a \leq r \leq b, \quad t > 0, \quad (12)$$

where  $s = \sqrt{\chi_1/\chi_2}$ ,  $\gamma_n$  are the dimensionless eigenvalues (rescaled separation constants) of the modified boundary-initial problem (2)–(6);  $C_n$ ,  $D_n$ ,  $E_n$  are the coefficients of eigenfunctions, and  $J_k(\dots)$ ,  $Y_k(\dots)$  are Bessel functions of the first and second kinds of order  $k$ .

Next, the eigenvalues of the modified problem (2)–(6) were determined. For this purpose, the continuity conditions (6a, 6b) and the boundary condition (5a) with respect to  $v_{it}(r, t)$  were used. After substituting the distributions (11)–(12) in (6a, 6b) and (5a) (for  $v_i(r, t) \rightarrow v_{it}(r, t)$ ), a homogeneous system of three equations with respect to unknown coefficients  $C_n$ ,  $D_n$ ,  $E_n$  was obtained

$$C_n J_0(\gamma_n) - D_n J_0(\gamma_n s) - E_n Y_0(\gamma_n s) = 0, \quad (13)$$

$$K C_n J_1(\gamma_n) - D_n J_1(\gamma_n s) - E_n Y_1(\gamma_n s) = 0, \quad (14)$$

$$D_n \left[ \frac{\vartheta J_0(p s \gamma_n)}{\gamma_n s} - J_1(p s \gamma_n) \right] + E_n \left[ \frac{\vartheta Y_0(p s \gamma_n)}{\gamma_n s} - Y_1(p s \gamma_n) \right] = 0, \quad (15)$$

where  $K = \lambda_1/(\lambda_2 s)$ ,  $\vartheta = \alpha a/\lambda_2$ ,  $p = b/a$ .

The system of equations shown above has a non-trivial solution if its main determinant is zero

$$\Delta(\gamma_n) = [J_0(\gamma_n)Y_1(s\gamma_n) - KJ_1(\gamma_n)Y_0(s\gamma_n)] \cdot \left[ \frac{\vartheta J_0(p s \gamma_n)}{\gamma_n s} - J_1(p s \gamma_n) \right] + [KJ_1(\gamma_n)J_0(s\gamma_n) - J_0(\gamma_n)J_1(s\gamma_n)] \cdot \left[ \frac{\vartheta Y_0(p s \gamma_n)}{\gamma_n s} - Y_1(p s \gamma_n) \right] = 0. \quad (16)$$

Relationship (16) constitutes an eigenvalue equation.

In addition, using the system of equations (13)–(15) given above, the number of unknown coefficients can be reduced. For this purpose, the first two equations, (13) and (14), were used. As a result, the coefficients  $D_n$ ,  $E_n$  were made dependent on  $C_n$ . So expressed coefficients  $D_n$ ,  $E_n$  were substituted in (12). After appropriate shortening of the notation, the following was obtained

$$v_{2t}(r, t) = \sum_{n=1}^{\infty} C_n Z_0(\gamma_n s r/a) e^{-\gamma_n^2 \frac{\chi_1}{a^2} t} \quad \text{for } a \leq r \leq b, \quad t > 0, \quad (17)$$

where

$$Z_k(\gamma_n s r/a) = H_n J_k(\gamma_n s r/a) + Q_n Y_k(\gamma_n s r/a), \quad (18)$$

$$H_n = \frac{J_0(\gamma_n)Y_1(s\gamma_n) - KJ_1(\gamma_n)Y_0(s\gamma_n)}{J_0(s\gamma_n)Y_1(s\gamma_n) - Y_0(s\gamma_n)J_1(s\gamma_n)}, \quad (19)$$

$$Q_n = \frac{KJ_0(s\gamma_n)J_1(\gamma_n) - J_0(\gamma_n)J_1(s\gamma_n)}{J_0(s\gamma_n)Y_1(s\gamma_n) - Y_0(s\gamma_n)J_1(s\gamma_n)}. \quad (20)$$

The form of equation (11) has not changed. The unknown coefficient  $C_n$  in (11), (17) still needs to be determined. For its determination, the initial conditions (10) were used. The substitution of distributions (11), (17) in (10) yields

$$\sum_{n=1}^{\infty} C_n J_0(\gamma_n r/a) = -v_{1s}(r) \quad \text{for } 0 \leq r \leq a, \quad (21)$$

$$\sum_{n=1}^{\infty} C_n Z_0(\gamma_n s r/a) = -v_{2s}(r) \quad \text{for } a \leq r \leq b. \quad (22)$$

Next, relationship (21) was multiplied by  $r \cdot (\lambda_1/\chi_1) \cdot J_0(\gamma_n r/a)$  and then integrated by sides in the interval of  $\langle 0, a \rangle$ . Similar operations were made for relationship (22), multiplying it by  $r \cdot (\lambda_2/\chi_2) \cdot Z_0(\gamma_n s r/a)$  and integrating in the interval of  $\langle a, b \rangle$ . Thus obtained relationships were added together. Subsequently, the condition of the orthogonality of radial coordinate eigenfunctions in multi-zone cylindrical systems (proved in [25])

was used

$$\frac{\lambda_1}{\chi_1} \int_0^a r J_0(\gamma_n r/a) J_0(\gamma_m r/a) dr + \frac{\lambda_2}{\chi_2} \int_a^b r Z_0(\gamma_n s r/a) Z_0(\gamma_m s r/a) dr = \begin{cases} 0 & \text{for } \gamma_n \neq \gamma_m, \\ \|N(m)\|^2 & \text{for } \gamma_n = \gamma_m, \end{cases} \quad (23)$$

where  $\|N(m)\|^2$  is the square of the norm, defined by formula (25). After calculating the relevant integrals obtained as a result of the above-mentioned operations and after making appropriate arrangement, abridgment and change  $m \rightarrow n$ , the  $C_n$  coefficient searched for was ultimately obtained

$$C_n = \frac{F_1(n) + F_2(n)}{\|N(n)\|^2}, \quad (24)$$

where

$$\|N(n)\|^2 = \frac{\lambda_1}{2\chi_1} a^2 [J_0^2(\gamma_n) + J_1^2(\gamma_n)] + \frac{\lambda_2}{2\chi_2} b^2 [Z_0^2(p s \gamma_n) + Z_1^2(p s \gamma_n)] - \frac{\lambda_2}{2\chi_2} a^2 [Z_0^2(s\gamma_n) + Z_1^2(s\gamma_n)], \quad (25)$$

$$F_1(n) = -\frac{\lambda_1}{\chi_1} \left\{ \frac{g_1 a^4}{2\lambda_1 \gamma_n^2} J_2(\gamma_n) + \frac{a^2}{\gamma_n} J_1(\gamma_n) \left[ \frac{g_2(b^2 - a^2)}{4\lambda_2} - \frac{(g_2 - g_1)a^2}{2\alpha b} + \frac{g_2 b}{2\alpha} - \frac{(g_2 - g_1)a^2}{2\lambda_2} \ln\left(\frac{b}{a}\right) \right] \right\}, \quad (26)$$

$$F_2(n) = \frac{\lambda_2}{\chi_2} \left[ \frac{g_2 b^2 a^2}{4\lambda_2 \gamma_n s} Z_1(s\gamma_n) - \frac{g_2 a^4}{4\lambda_2 \gamma_n s} Z_1(s\gamma_n) - \frac{g_2 b^2 a^2}{2\lambda_2 \gamma_n^2 s^2} Z_2(s\gamma_n b/a) + \frac{g_2 a^4}{2\lambda_2 \gamma_n^2 s^2} Z_2(s\gamma_n) - \frac{(g_2 - g_1)a^4}{2\lambda_2 \gamma_n s} Z_1(s\gamma_n) \ln\left(\frac{b}{a}\right) \right] + \frac{\lambda_2}{\chi_2} \left\{ \frac{(g_2 - g_1)a^4}{2\lambda_2 \gamma_n^2 s^2} [Z_0(s\gamma_n) - Z_0(s\gamma_n b/a)] + \frac{g_2(b^2 - a^2) + g_1 a^2}{2\alpha b} \left[ \frac{a^2}{\gamma_n s} Z_1(s\gamma_n) - \frac{ab}{\gamma_n s} Z_1(s\gamma_n b/a) \right] \right\}, \quad (27)$$

where  $g_1$  and  $g_2$  are expressed with formulas (3).

Finally, after considering (1), (7) and (11), (17), space-time variable heating curves for the conductor were obtained

$$T_1(r, t) = T_s + v_{1s}(r) + \sum_{n=1}^{\infty} C_n J_0(\gamma_n r/a) e^{-\gamma_n^2 \frac{\chi_1}{a^2} t} \quad \text{for } 0 \leq r \leq a, \quad t > 0, \quad (28)$$

$$T_2(r, t) = T_s + v_{2s}(r) + \sum_{n=1}^{\infty} C_n Z_0(\gamma_n s r/a) e^{-\gamma_n^2 \frac{\chi_1}{a^2} t}$$

for  $a \leq r \leq b$ ,  $t > 0$ , (29)

where  $v_{1s}(r)$ ,  $v_{2s}(r)$  are given by formulas (8), (9), the coefficient  $C_n$  is given by relationship (24), while taking into account (25)–(27), whereas  $\gamma_n$  is determined from (16). The influence of wind speed is hidden in the total heat transfer coefficient  $\alpha$  (5a), (5b).

## 5. STATIONARY TEMPERATURE PROFILES, STEADY-STATE CURRENT RATINGS, LOCAL TIME CONSTANTS OF THE ACCR LINE

Stationary temperature distributions are determined from (28)–(29) at  $t \rightarrow \infty$ . As a result, this comes down to zeroing the exponential functions, or omitting the series in (28)–(29)

$$T_i(r, t \rightarrow \infty) = T_s + v_{is}(r). \quad (30)$$

One of the most important parameters of conductors is the steady-state current rating (or current rating capacity)  $|I_{cr}|$ . The composite Al–Al<sub>2</sub>O<sub>3</sub> is more thermally stable than the Al–Zr alloy (the emergency use temperatures are, respectively, 300°C and 240°C, [26]). For this reason, the temperature field generated by the current  $|I_{cr}|$  should be examined in the most poorly cooled place of the Al–Zr braid (i.e., for  $r = a$ ). From (30), the following results for  $i = 2$

$$T_s + v_{2s}(r = a, |I_{cr}|) = T_{\max}, \quad (31)$$

where  $T_{\max}$  denotes the maximum operating temperature (or the sustained maximum temperature). Then, (3) was substituted in (9) and, in turn, (9) in (31). Appropriate transformation yielded the following

$$|I_{cr}| = \sqrt{\frac{I_{cr1}}{I_{cr1}}}, \quad (32)$$

where:

$$I_{cr1} = 4\pi\alpha\lambda_2 b (T_{\max} - T_s) (b^2 - a^2) (k_1 n_1 \rho_1 S_2 + k_2 n_2 \rho_2 S_1)^2,$$

$$I_{cr1} = k_1 k_2 n_1 n_2 \rho_1 \rho_2 \left\{ k_1 n_1 \rho_1 S_2 \left[ (b^2 - a^2) (\alpha b + 2\lambda_2) - 2a^2 \alpha b \ln\left(\frac{b}{a}\right) \right] + 2k_2 n_2 \rho_2 S_1 (b^2 - a^2) \left[ \lambda_2 + b\alpha \ln\left(\frac{b}{a}\right) \right] \right\},$$

where, to simplify the notation, it is assumed that  $\alpha = \alpha(U)$  (5b).

Another important parameter of thermal field dynamics is the time constant of the conductor. To determine it, the local time constant criterion,  $\tau_i(r)$ , was used. This is done by approximating the dynamic of each point using the first order lag. The step response of such an object is well known and is expressed by the formula

$$T_i(r, t) = T_i(r, t \rightarrow \infty) \{1 - \exp[-t/\tau_i(r)]\} + T_i(r, t = 0) \exp[-t/\tau_i(r)], \quad (33)$$

where  $i = 1, 2$ . Formula (33) results in the relationship below [27, 28]

$$\tau_i(r) = \int_0^{\infty} \frac{T_i(r, t) - T_i(r, t \rightarrow \infty)}{T_i(r, t = 0) - T_i(r, t \rightarrow \infty)} dt. \quad (34)$$

After substituting distributions (28), (29) and (30) in (34) and then performing integration, the following were ultimately obtained

$$\tau_1(r) = \frac{a^2 \sum_{n=1}^{\infty} C_n J_0(\gamma_n r/a) / \gamma_n^2}{\chi_1 \sum_{n=1}^{\infty} C_n J_0(\gamma_n r/a)}, \quad \text{for } 0 \leq r \leq a, \quad (35)$$

$$\tau_2(r) = \frac{a^2 \sum_{n=1}^{\infty} C_n Z_0(s\gamma_n r/a) / \gamma_n^2}{\chi_1 \sum_{n=1}^{\infty} C_n Z_0(s\gamma_n r/a)}, \quad \text{for } a \leq r \leq b. \quad (36)$$

Using the local time constant, it is possible, e.g., to estimate the transient state duration and the temperature change rapidity at a given point of the system.

## 6. COMPUTATION EXAMPLES

The heating curves (28), (29) and other parameters of the ACCR line were computed using a software program developed in the Mathematica 10.4 environment [29]. The material parameters were averaged in the temperature variation interval. The following data were adopted [2, 10, 18, 21, 23, 26]:

$$\begin{aligned} a &= 0.006 \text{ m}, & b &= 0.01795 \text{ m}, \\ c_1 &= 906.6 \text{ J/(kgK)}, & c_2 &= 984.2 \text{ J/(kgK)}, \\ \mu_1 &= 2502.9 \text{ kg/m}^3, & \mu_2 &= 2030.2 \text{ kg/m}^3, \\ \lambda_1 &= 68.7 \text{ W/(mK)}, & \lambda_2 &= 160.15 \text{ W/(mK)}, \\ S_1 &= 85 \cdot 10^{-6} \text{ m}^2, & S_2 &= 676 \cdot 10^{-6} \text{ m}^2, \\ \varepsilon &= 0.5, & n_1 &= n_2 = 1.02, \\ f &= 50 \text{ Hz}, & k_1 &= 1.0001, \quad k_2 = 1.026, \\ T_a &= 40^\circ\text{C}, & T_s &= 55^\circ\text{C}, \quad T_{\max} = 210^\circ\text{C}, \\ \rho_1 &= 11.8 \cdot 10^{-8} \Omega\text{m}, & \rho_2 &= 3.89029 \cdot 10^{-8} \Omega\text{m}. \end{aligned} \quad (37)$$

The  $f_3$ ,  $f_4$  functions (5b) were determined based on formulas presented in [10], [21] – Table 3, respectively.

The graph of the relationship of the steady-state current rating  $|I_{cr}|$  as a function of wind speed has been plotted based on formula (32), assuming that  $T_{\max} = 210^\circ\text{C} = \text{const}$ , and it is shown in Fig. 2. This results in the value of  $|I_{cr}| = 2359.8 \text{ A}$  for the mains frequency  $f = 50 \text{ Hz}$ ,  $U = 0.6 \text{ m/s}$ ,  $\Theta = 90^\circ\text{C}$  (manufacturer's conditions [2]).

Figure 3 represents the effect of variation in wind speed  $\{U = 0 \text{ m/s}, 0.6 \text{ m/s}, 1 \text{ m/s}, 2 \text{ m/s}, 4 \text{ m/s}, 10 \text{ m/s}\}$  on the heating curves at the point  $r = a$  (with the identical root-mean-square value of  $|I_{cr}| = 2359.8 \text{ A}$  and wing angle  $\Theta = 90^\circ\text{C}$  in each

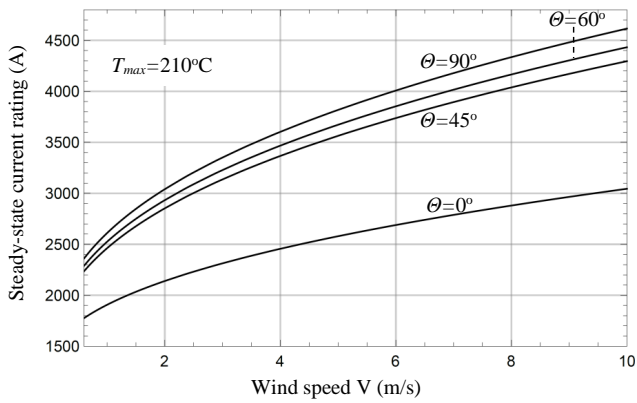


**Fig. 2.** Steady-state current rating as a function of wind speed for varying angles of attack  $\Theta$  (assuming  $T_{\max} = 210^{\circ}\text{C} = \text{const}$ )

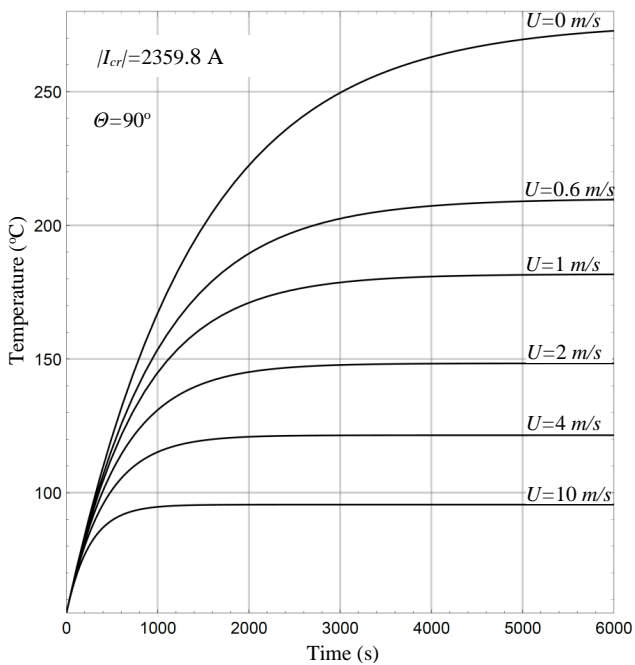


**Fig. 3.** Heating curves for  $r = a$  at a current of  $|I_{\text{cr}}| = 2359.8 \text{ A}$  for selected wind speeds (with an angle of attack of  $\Theta = 90^{\circ}$ )

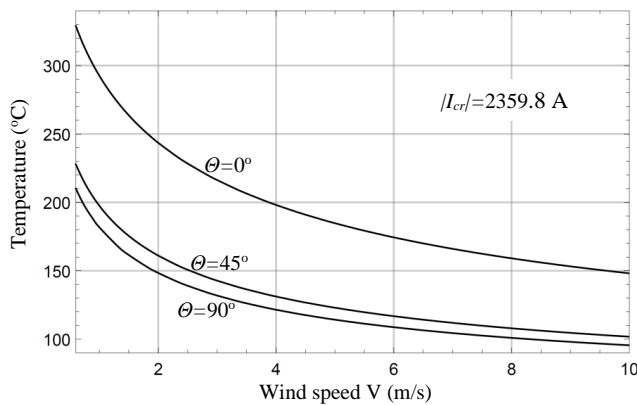


**Fig. 4.** Variation in stationary temperature  $T_{s2}(r = a)$  as a function of wind speed for varying angles of attack  $\Theta$

case). It can be noticed that only for  $U = 0.6 \text{ m/s}$  is the accurate maximum operating temperature value of  $T_{\max} = 210^{\circ}\text{C}$  attained. The upper curve illustrates the heating of the line with free convection ( $U = 0 \text{ m/s}$ ). Figure 4, in turn, shows variation in stationary temperature (i.e., (29) at  $t \rightarrow \infty$ ) as function of wind speed and at point  $r = a$  (with a constant root-mean-square value of  $|I_{\text{cr}}| = 2359.8 \text{ A}$ ). Figure 5 shows the difference in the heating curves in the center and on the surface of the system, respectively,  $T_1(r = 0, t) - T_2(r = b, t)$ , for selected wind speeds (with constant parameters  $|I_{\text{cr}}| = 2359.8 \text{ A}$  and  $\Theta = 90^{\circ}\text{C}$ ). The last determined parameter is the thermal time constant of the conductor, calculated from relationships (35), (36). Its diagram as a function of wind speed for varying angles of attack is shown in Fig. 6.

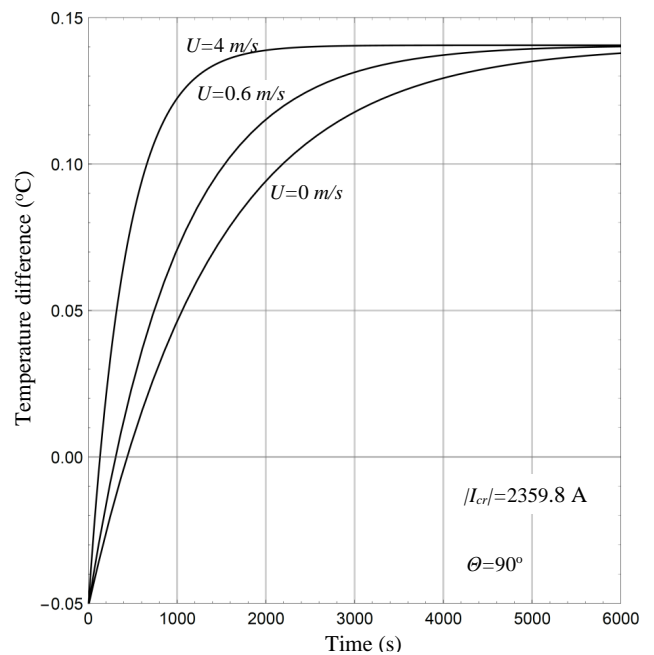


**Fig. 5.** Differences in the heating curves in the center and on the surface of the system, respectively,  $T_1(r = 0, t) - T_2(r = b, t)$ , for selected wind speeds (with an angle of attack of  $\Theta = 90^{\circ}$  and a current of  $|I_{\text{cr}}| = 2359.8 \text{ A}$ )

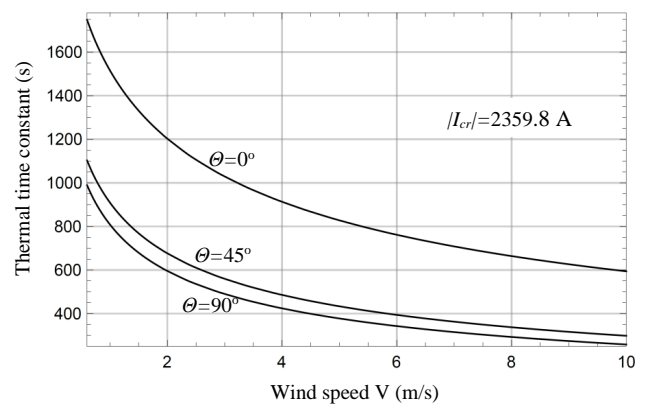


**Fig. 6.** Dependence of the time constant on the wind speed for varying angles of attack

## 7. NUMERICAL VERIFICATION OF CALCULATIONS

To verify the correctness of formulas (28), (29), the boundary-initial problem (2)–(6) was solved again, but this time using a finite-element (FE) method [14, 15, 30]. The same simplifying assumptions as in the analytical method were adopted. The FE method forms the basis of the professional NISA v.16 software program [31], which was used for numerical analysis. Next, the relative differences in temperature increments were calculated from the formula

$$\delta_{Ti} = 100\% \frac{v_i(r,t) - v_i^{(FE)}(r,t)}{v_i(r,t)}, \quad \text{for } i = 1, 2, \quad (38)$$

where  $v_i(r,t)$  is the temperature increase distribution obtained by the variables separation method in the  $i$ -th zone, while  $v_i^{(FE)}(r,t)$  represents the temperature increase distribution calculated by the finite-element method in the  $i$ -th zone. Figure 7 illustrates relationship (38) at the point  $r = a$  of the conductor. At the remaining points of the line, the differences (38) for a given wind speed take on values almost identical to those at point  $r = a$ . For the sake of the legibility of the graph, the analysis is limited to the case  $U = 0.6$  m/s. It should be added that the integrals in formula (23) were also calculated both analytically and numerically. A full consistency of the results was obtained.

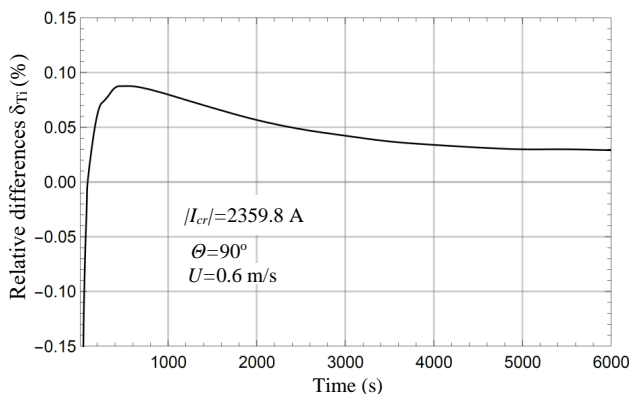


**Fig. 7.** Relative difference (38) in the temperature increments at point  $r = a$ , determined by the variable-separation and finite-element methods for  $|I_{cr}| = 2359.8$  A,  $\Theta = 90^\circ$  C,  $U = 0.6$  m/s

## 8. CONCLUSIONS

The study modeled influence of the wind speed on thermal characteristics of the ACCR line. Heating curves, steady-state current ratings, time constants and stationary temperature profiles were discussed. The following conclusions can be drawn from the analysis:

- The increase in wind speed causes an increase in the amount of heat given up by the line. Therefore, maintaining the same operating temperature  $T_{max}$  requires increasing the current  $|I_{cr}|$  (Fig. 2). In turn, increasing the angle  $\Theta$  (between the conductor axis and the wind direction) from  $0^\circ$  to  $90^\circ$  results in an increase in the Nusselt number [21] – Table 3, and thus an increase in the convection heat transfer coefficient,  $\alpha_c$ . Therefore, with the cross-air flow ( $\Theta = 90^\circ$ ),

the condition of  $T_{max} = \text{const}$  forces the flow of the largest current  $|I_{cr}|$  for a given wind speed (Fig. 2).

- The increase in wind speed at a constant value of steady-state current rating ( $|I_{cr}| = \text{const}$ ) causes a drop in steady-state temperature (Fig. 3). This is fully confirmed by Fig. 4. The increase in wind speed also shortens the duration of the transient state (Fig. 3). This correlates well with Fig. 6 (the duration of the transient state is estimated to be five times the time constant value). It follows from the previous bullet point that the heat transfer coefficient attains the greatest value for  $\Theta = 90^\circ$ . So, for  $\Theta = 90^\circ$ , the most intensive heat exchange occurs between the conductor and the environment at a given wind speed. This explains the lowest position of the  $\Theta = 90^\circ$  curves in Fig. 4 and Fig. 6.
- It is assumed that  $t_1$  represents the moment of time, for which  $T_1(r = 0, t_1) = T_2(r = b, t_1)$  occurs. Figure 5 shows that in the range  $< 0, t_1$  the temperature of the line surface ( $r = b$ ) is slightly higher than the line center ( $r = 0$ ). This results from two causes: a) the large value of current flowing through the braid  $|I_2| \approx 0.96|I_{cr}|$ , b) the thermal inertia of the braid which, within the short time  $t_1$ , “will not be able to give up the heat” (for  $0 \leq t < t_1$  the surface  $r = b$  behaves like an adiabat). For  $t > t_1$ , the direction of the phenomenon changes and there occurs  $T_1(r = 0, t) > T_2(r = b, t)$  (Fig. 5) (the braid gives up the heat to the environment and, while restraining its outflow from the core). Lowering the wind speed will impair the cooling of the brain, thus increasing the time  $t_1$  (Fig. 5). It can be noted that the isothermal model [4] precludes the investigation of the described phenomenon.
- In a transient state, the relative difference (38) changes from  $-0.15\%$  to  $0.09\%$  and after passing on to a steady state, it decreases to  $0.03\%$  (Fig. 7). Such small values are achieved in the most unfavorable position of  $r = a$  (i.e., on the border between different materials, where the accuracy of numerical computations is the lowest). This means that the finite-element method has confirmed the result obtained by the variables separation method.
- The use of the analytical model was advantageous for the following reasons:
  - the discretization of the area and time is unnecessary,
  - summing the finite number of the terms of series (28), (29) is very simple. At the same time, no limitations on the computer memory are relevant. Numerical methods are much more complex (e.g., numerical integration with respect to time, assembling a matrix, solving large-scale matrix equations, etc., are required). In FEM, the size of the system’s matrix is critically limited by the computer memory,
  - in the adopted criterion of truncation series (28), (29), the solution provides a comparable level of error at all points of the region (in FEM, a non-uniform distribution of error occurs, which is dependent on the grid construction and material structure),
  - solutions of (28), (29) provide a minimum error value. It is limited either by the precision of the floating point arithmetic or by the arbitrarily adopted criterion of trun-



cation series (28), (29) (in FEM, the error is greater by several orders of magnitude than the level of precision of floating point arithmetic).

According to the authors' best knowledge, the effect of wind speed on the thermal characteristics of the ACCR line has not been studied so far. The earlier bullet points show that the determined analytically characteristics have a very good physical interpretation. The correctness of the paper's results is proved also by the positive verification of the analytical considerations using numerical means.

The presented methodology enables additionally the analysis of the effect of other factors on the thermal characteristics of the ACCR line (such as infrared emissivity,  $\epsilon$ , or ambient air temperature,  $T_a$ ). The analytical method will be also effective in mathematical modelling of modern lines of a different type (such as, e.g., ACCC, ACSS, TACIR and TACSR).

## ACKNOWLEDGEMENTS

The paper was prepared in Technical University of Białystok within a framework of the project WZ/WE-IA/2/2020 sponsored by the Ministry of Science and Higher Education.

## REFERENCES

- [1] J. Hunt, *Advanced technology high-temperature conductors, Electric power generation, transmission and distribution*. USA: CRC Press, 2012, ch. 24.
- [2] 3M Aluminum Conductor Composite Reinforced (ACCR), Technical Summary for Common Constructions and Sizes. Metric Units, Electrical Markets Division, 3M High Capacity Conductors, St. Paul, MN, USA, 2009.
- [3] M. Bockarjova and G. Andersson, "Transmission Line Conductor Temperature Impact on State Estimation Accuracy," in *Proc. of Power Tech. IEEE*, Lausanne, 2007, pp. 701–706.
- [4] T. Knych, *Overhead power lines. Theory – Materials – Applications*. Kraków AGH: Publishing House, 2010 [in Polish].
- [5] J. Gentle *et al.*, "Concurrent wind cooling in power transmission lines," in *Western Energy Policy Research Conf.*, Boise, Idaho, 2012.
- [6] Y.Q. Ding *et al.*, "The effect of calculated wind speed on the capacity of dynamic line rating," in *IEEE International Conference on High Voltage Engineering and Application*, 2016, pp. 1–5.
- [7] H.M. Goh and N.E. Chin, "Critical aging segments of power transmission line," *Am. J. Appl. Sci.*, vol. 6, pp. 340–351, 2013.
- [8] IEEE Std. 738-2012, IEEE Standard for calculating the current-temperature relationship of bare overhead conductors, IEEE Standard Association, Piscataway Township, NJ, USA, 2013.
- [9] CIGRE Working Group B2.42, Guide for thermal rating calculations of overhead lines, Technical Brochure 601, CIGRE, Paris, France, 2014.
- [10] F. Incropera, D. De Witt, T. Bergman, and A. Lavine, *Introduction to heat transfer*. USA: John Wiley&Sons, 2007.
- [11] U.V. Bourgsdorf and L.G. Nikitina, "Heating of conductors, their thermal endurance and increase in transmission line capacity," in *CIGRE Conference*, Paris, 1980, Paper 22–04.
- [12] J. Fu., S. Abbott, B. Fox, D.J. Marrow, and S. Abdelkaber, "Wind cooling effect on dynamic overhead line ratings," in *45th International Universities Power Engineering Conference UPEC*, Cardiff, UK, 2010.
- [13] J.D. Hoffman, "On thermal aging prevention in polymer core composite conductor rods," PhD Thesis, University of Denver, USA, 2015. [Online] Available: <https://digitalcommons.du.edu/etd/1066> [Accessed: 17 Feb. 2021].
- [14] P. Nithiarasu, R.W. Lewis, and K.N. Seetharamu, *Fundamentals of the finite element method for heat and mass transfer*. UK: John Wiley & Sons, 2016.
- [15] S. Berhausen and S. Paszek, "Use of the finite element method for parameter estimation of the circuit model of a high power synchronous generator", *Bull. Pol. Acad. Sci. Tech. Sci.*, vol. 63, no. 3, pp. 575–582, 2015, doi: [10.1515/bpats-2015-0067](https://doi.org/10.1515/bpats-2015-0067).
- [16] L.C. Evans, *Partial differential equations*. Rhode Islands: American Mathematical Society, 2010.
- [17] M.J. Latif, *Heat Conduction*. Haidelberg: Springer-Verlag, 2009.
- [18] D.A. Nield and A. Bejan, *Convection in porous media*. New York: Springer-Verlag, 2013.
- [19] D.C. Lawry and J.R. Daconti, "Overhead line thermal rating calculation based on conductor replica method," in *2003 IEEE PES Transmission and Distribution Conference and Exposition*, pp. 880–885, 2003.
- [20] P. Kubek and E. Siwy, "Analysis methods of HTLS conductors in terms of mechanical and thermal criteria," *Acta Energ.*, vol. 1, pp. 75–82, 2013.
- [21] R.T. Coneybeer, W.Z. Black, and R.A. Bush, "Steady – state and transient ampacity of bus bar," *IEEE Trans. Power Deliver.*, vol. 9, pp. 1822–1829, 1994.
- [22] D.W. Hahn and M.N. Ozisik, *Heat Conduction*. New Jersey: John Wiley & Sons, 2012.
- [23] G.J. Anders, *Rating of electric power cables: ampacity computations for transmission, distribution and industrial application*. New York: McGraw-Hill Professional, 1997.
- [24] V.T. Morgan, "The current distribution, resistance and internal inductance of linear power system conductors – a review of explicit equations," *IEEE Trans. Power Deliv.*, vol. 38, pp. 1252–1262, 2013.
- [25] S. Singh, P.K. Jain and Rizwan-uddin, "Analytical solution to transient heat conduction in polar coordinates with multiple layers in radial direction," *Int. J. Therm. Sci.*, vol. 47, pp. 261–273, 2008.
- [26] 3M Aluminium Composite Reinforced, Technical Notebook. Conductor and Accessory Testing, Composite Conductor Program, 3M High Capacity Conductors, St. Paul, MN, USA, 2003.
- [27] A. Avramescu, "Eindringzeit des elektromagnetischen Feldes und des Wärmefeldes in Leiter," *Elektrotechnische Zeitschrift-A*, vol. 91, pp. 235–238, 1970.
- [28] A. Brykalski, "Über die Eindringzeit des elektromagnetischen Feldes in Leiter," *Archiv für Elektrotechnik*, vol. 68, pp. 299–304, 1985.
- [29] Wolfram Research, Inc., *Mathematica*, Illinois: Wolfram Research Inc., 2021.
- [30] A. Piekarczyk, "Test-supported numerical analysis for evaluation of the load capacity of thin-walled corrugated profiles," *Bull. Pol. Acad. Sci. Tech. Sci.*, vol. 65, no. 6, pp. 791–798, 2017, doi: [10.1515/bpats-2017-0087](https://doi.org/10.1515/bpats-2017-0087).
- [31] Manuals for NISA v.16, *NISA Suite of FEA Software (CD-ROM)*, Cranes Software, Inc. Troy, MI, USA, 2008.